ELSEVIER

Chemical Engineering Science 63 (2008) 1117–1130

Chemical Engineering Science

www.elsevier.com/locate/ces

Modelling the effect of temperature and time on the performance of a copper electrowinning cell based on reactive electrodialysis

L. Cifuentes[a,*], J.M. Casas[a], J. Simpson[b]

[a]*Departamento de Ingeniería de Minas, Universidad de Chile, Tupper 2069, Santiago, Chile*
[b]*Departamento de Ingeniería Metalúrgica, Universidad de Santiago, Ecuador 3659, Santiago, Chile*

Received 14 September 2006; received in revised form 26 October 2007; accepted 3 November 2007
Available online 12 November 2007

Abstract

A temperature- and time-dependent mathematical model for the operation of a laboratory-scale copper electrowinning cell based on reactive electrodialysis (RED) has been developed. The model is zero-dimensional. The cathodic reaction was copper electrodeposition and the anodic reaction was ferrous to ferric ion oxidation. The catholyte was aqueous cupric sulphate and the anolyte was aqueous ferrous sulphate, both in sulphuric acid. Catholyte and anolyte were separated by an electrodialytic anion membrane. The model predicts the effect of temperature and time on: (a) cathodic and anodic kinetics, (b) speciation of catholyte and anolyte, (c) transport phenomena in the electrolytes and (d) ion transport through the membrane. Model calibration and validation were carried out. Its predictions are in good agreement with experiments for: amount of deposited copper, amount of produced Fe(III) species, cell voltage and specific energy consumption.

Keywords: Mathematical modelling; Reaction engineering; Electrochemistry; Kinetics; Reactive electrodialysis; Speciation

1. Introduction

1.1. Overcoming the limitations of conventional copper electrowinning cells

The limitations of the operation of conventional copper electrowinning cells (low mass transfer rate, low specific cathode surface area, high cell voltage, air contamination with acid mist) have been discussed by a number of authors (Cifuentes et al., 2004a, 2005 and references therein). In order to overcome such limitations, several alternative cells have been developed. One of them, the reactive electrodialysis (RED) cell uses two electrolytes (anolyte and catholyte), while conserving a conductive path between them by means of an anion membrane (Cifuentes et al., 2004a, b). A basic model has been developed for the operation of an RED cell at 50 °C (Cifuentes et al., 2007); however, a far more useful model would allow for temperature variations, which are crucial to the electrochemical kinetics and transport phenomena in the electrolytes and membrane, and therefore, to the value of significant operation parameters such as cell voltage and specific energy consumption.

1.2. Prospects of RED cells

Published and unpublished work carried out by the authors regarding copper electrowinning cells based on RED has shown that these designs remain promising, basically due to:

(a) Their capability to reduce the specific energy consumption from about 2 kWh/kg for conventional EW to less than 0.6 kWh/kg for RED cells at similar cell current densities. This represents a massive 70% reduction in electrical energy cost.
(b) The high price of the ferric compounds produced in the RED anolyte compared to the ferrous reactants. For instance, the price of analytical grade ferric sulphate ($Fe_2(SO_4)_3 \cdot H_2O$) is about 10 times greater than the price of analytical grade ferrous sulphate ($FeSO_4 \cdot 7H_2O$). Technical grade ferric sulphate is still about 6 times the

* Corresponding author. Tel.: +56 2 978 4510; fax: +56 2 672 3504.
E-mail address: luicifue@cec.uchile.cl (L. Cifuentes).

0009-2509/$ - see front matter © 2007 Elsevier Ltd. All rights reserved.
doi:10.1016/j.ces.2007.11.004

price of analytical grade ferrous sulphate. Ferric sulphate can be obtained from the spent anolyte by increasing acidity or temperature, both of which tend to saturate the solution, thereby favouring crystallization (Casas et al., 2005a).

The development of EW-RED cells is still being carried out at lab-scale. A pilot-scale stage is a must in order to determine the building, operation and operation parameters of a potential industrial plant. In summary, there is a fair amount of development work to be done before RED cells become an industrial reality. The present model is meant to assist this development effort by quantifying the effect of temperature on important production parameters such as production rate, cell voltage and specific energy consumption. In order to aid the design of RED cells, data provided by the present model would have to be fed into 2-D and 3-D models (currently being developed by finite element methods) which would quantify the effect of geometry changes (cell size and shape, cathode–anode distance, electrolyte flow patterns and so on) on the resulting copper production.

1.3. Objective

The objective of the present work is to develop and validate a temperature- and time-dependent mathematical model for the operation of a copper electrowinning cell based on RED. This is achieved by including submodels for the temperature dependence of the speciation, the electrochemical kinetics and electrolyte properties such as density, viscosity and electrical conductivity. The model assumes that temperature does not vary with time.

This model does not provide solutions for the spatial distribution of variable values, i.e., it is zero-dimensional. Instead, it provides overall solutions for properties such as copper production, Fe(III) species production, cell voltage and specific energy consumption, all as a function of temperature and cell operation time. As stated above, models which do provide spatial distributions in 2-D and 3-D are currently being developed.

2. Experimental

2.1. Dependence on temperature of transport properties

The dependence on temperature of the density, viscosity and electrical conductivity of the studied electrolytes was determined by experiment in the 30–60 °C range. Density was measured with a glass pycnometer, viscosity with a glass viscosimeter and electrical conductivity with a Hanna 9835 conductivity unit. Effective diffusivities for relevant ions were determined by a procedure given below.

2.2. RED cell

To determine the effect of temperature on the performance of the RED cell, experiments were carried out in a lab-scale RED reactor (Fig. 1). The cell is made of acrylic and it consists of two compartments. The first one contains anode and anolyte and the second one, cathode and catholyte. Both electrolytes were recirculated to separate 1 L tanks by means of Watson-Marlow 505 S peristaltic pumps at a flow rate of 700 cm^3/min. The effective volume of catholyte and anolyte in the compartments was 275 cm^3 each, while their total volume was 725 cm^3 each. Temperature was kept constant by a Julabo thermostatic bath.

The cathode was a 4 cm^2 copper sheet (its back face masked with Teflon tape) and the anode was a 4 cm^2 platinum sheet, equally masked. The cathode–anode distance was 10 mm. An Ionac MA3475 anion membrane, whose aim was to hinder the passage of cations between the electrolytes, was placed in a 2 cm × 2 cm window cut in the acrylic plates between

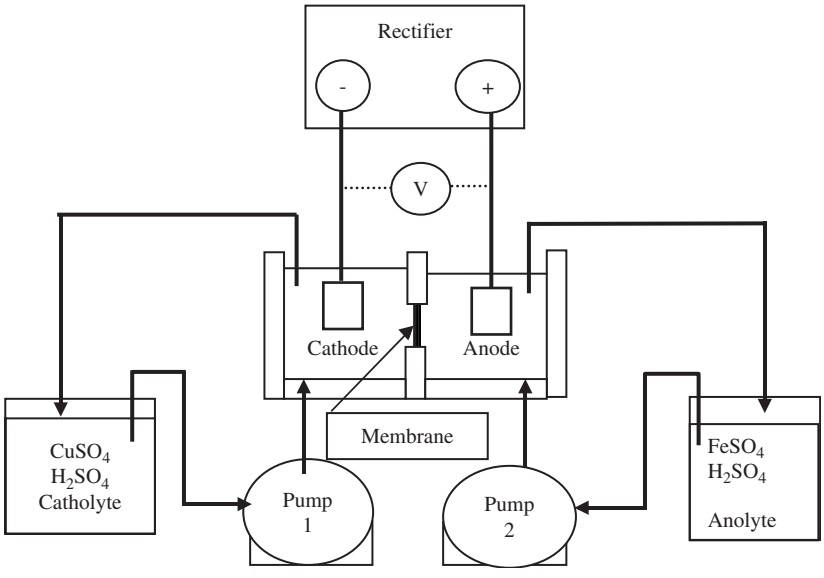

Fig. 1. Experimental setup, showing RED cell, rectifier and recirculation tanks for catholyte and anolyte.

Table 1
Operation parameters for RED cell runs

Parameters	Values
Cell current density	300, 450 and 600 A/m^2
Anolyte composition	190 g/L H_2SO_4; 60 g/L Fe (II) (as $FeSO_4 \cdot 7H_2O$)
Catholyte composition	190 g/L H_2SO_4; 30 g/L Cu(II) (as $CuSO_4 \cdot 5H_2O$)
Electrolyte temperature	30, 40, 50, 60 °C
Electrolyte flow rate	700 cm^3/min
Anode material	Platinum sheet
Cathode material	Copper sheet
Interelectrode distance	10 mm
Electrode surface area	$A_m = A_a = A_c = 0.0004\,m^2$

the compartments. The membrane was kept in place by two 2 mm thick rubber seals. The anolyte composition was 190 g/L H_2SO_4 and 60 g/L Fe(II) (as $FeSO_4 \cdot 7H_2O$). The catholyte composition was 190 g/L H_2SO_4 and 30 g/L Cu(II) (as $CuSO_4 \cdot 5H_2O$). Deionized water and analytical grade chemicals were used for all the experiments in this work.

2.3. RED cell runs

At 30, 40, 50 and 60 °C 4 h runs were carried out in the above-described RED cell in order to determine the dependence on temperature and time of: (a) the cell voltage; (b) Cu(II) concentration in the catholyte; and (c) Fe(II) and Fe(III) concentrations in the anolyte. The cell was operated at cell current densities of 300, 450 and 600 A/m^2 provided by a 2 A, 30 V rectifier. The cell voltage was continuously monitored. Copper and iron were analysed by atomic absorption spectroscopy. The deposited copper mass was also measured.

Operation parameters for the RED cell are in Table 1.

All reported electrode potentials are referenced to the standard hydrogen electrode (SHE).

3. Modelling

The developed model describes and quantifies the dependence on temperature and time of the anodic and cathodic electrode kinetics, ion transport through the membrane and the speciation for the Cu(II)–H_2SO_4–H_2O catholyte and the Fe(II)–Fe(III)–H_2SO_4–H_2O anolyte.

3.1. Electrolyte speciation

Tables 2 and 3 present the components, species and main chemical reactions for catholyte and anolyte.

The speciation model consists of a set of equations for the mass balance of the system's components and the equilibrium relationships for all the species present in the studied systems (Casas et al., 2000, 2005a). The activity for each species is obtained from the equilibrium constants of formation (K_f^0) and mean activity coefficients ($\gamma_\pm$) calculated by an

Table 2
Speciation model for the anolyte: Fe(II)–Fe(III)–H_2SO_4–H_2O

Species	Components			
	H^+	SO_4^{2-}	Fe^{2+}	Fe^{3+}
HSO_4^-	1	1	0	0
$FeSO_{4(aq)}$	0	1	1	0
$FeH(SO_4)_{2(aq)}$	1	2	0	1
$Fe(SO_4)_2^-$	0	2	0	1
$FeSO_4^+$	0	1	0	1

Table 3
Speciation model for the catholyte: Cu–H_2SO_4–H_2O

Species	Components		
	H^+	SO_4^{2-}	Cu^{2+}
HSO_4^-	1	1	0
$CuSO_{4(aq)}$	0	1	1

extended Debye–Hückel equation first proposed by Helgeson (1969):

$$\log \gamma_{\pm j} = -\frac{A_\gamma z_j^2 \sqrt{I_\gamma}}{1 + r_j B_\gamma \sqrt{I_\gamma}} + \dot{B} \cdot I_\gamma. \quad (1)$$

Unlike previous versions of the Debye–Hückel equation, which only allowed predictions of activity coefficients for dilute solutions (up to 0.1 M), the extended equation (Eq. (1)) allows the prediction of activity coefficients for concentrated solutions such as those used in the present work (about 3.0 M) and, in the case of simpler solutions, for even higher concentrations. The applicability of this equation has been verified in the studied systems up to 3 M concentrations (Casas et al., 2005a, b).

Mass balance equations for anolyte and catholyte in the studied systems are as follows (Casas et al., 2000, 2005a; Cifuentes et al., 2002):

For the catholyte:

$$\mathrm{Cu(II)} = [Cu^{2+}] + [CuSO_4(aq)] + [CuHSO_4^+], \quad (2)$$

$$SO_4^{2-}(\mathrm{tot}) = [SO_4^{2-}] + [HSO_4^-] + [CuHSO_4^+] + [CuSO_4(aq)], \quad (3)$$

$$\mathrm{H(tot)} = 2[H_2O] + [H^+] + [HSO_4^-] + [CuHSO_4^+]. \quad (4)$$

For the anolyte:

$$\mathrm{Fe(II)} = [Fe^{2+}] + [FeSO_4(aq)], \quad (5)$$

$$\mathrm{Fe(III)} = [Fe^{3+}] + [FeSO_4^+] + [Fe(SO_4)_2^-] + [FeH(SO_4)_2(aq)], \quad (6)$$

$$\mathrm{H(tot)} = [H_2O] + [H^+] + [HSO_4^-] + [FeH(SO_4)_2^0], \quad (7)$$

$$SO_4^{2-}(\mathrm{tot}) = [SO_4^{2-}] + [HSO_4^-] + [FeSO_4^+] + [FeSO_4(aq)] + 2[Fe(SO_4)_2^-] + 2[FeH(SO_4)_2^0]. \quad (8)$$

In order to establish the temperature dependence of the speciation, values of the equilibrium constants of formation at various temperatures were obtained from the literature (Cifuentes et al., 2006). The parameters used in Eq. (1) are given in Casas et al. (2000).

3.2. Electrode kinetics

Possible electrode reactions are:

At the anode:

$$Fe^{2+} \rightarrow Fe^{3+} + e \quad \text{(main reaction)}, \tag{9}$$

$$2H_2O \rightarrow O_2 + 4H^+ + 4e \quad \text{(secondary reaction)}. \tag{10}$$

At the cathode:

$$Cu^{2+} + 2e \rightarrow Cu^0 \quad \text{(main reaction)}, \tag{11}$$

$$2H^+ + 2e \rightarrow H_2 \quad \text{(secondary reaction)}. \tag{12}$$

If an undesired transport of ferric ions through the anion membrane takes place, then the additional cathodic reaction

$$Fe^{3+} + e \rightarrow Fe^{2+} \tag{13}$$

would have the effect of reducing the cathodic current efficiency.

For the main reactions, the current densities are calculated by expressions for mixed control derived from Butler–Volmer and Fick equations (Bockris and Reddy, 2000). For the cathodic reaction:

$$|i_c| = \frac{i^b_{0,c}|i_{L,c}|}{i^b_{0,c} + |i_{L,c}| \exp\left(\dfrac{\alpha_c F}{GT}\eta_c\right)} \tag{14}$$

and for the anodic reaction:

$$i_a = \frac{i^b_{0,a} i_{L,a}}{i^b_{0,a} + i_{L,a} \exp\left(\dfrac{-\alpha_a F}{GT}\eta_a\right)}. \tag{15}$$

In Eqs. (14) and (15), due to the fact that the reactions are under mixed control, the overpotentials include the effects of both charge transfer and mass transfer.

Taking into account that the exchange current density may be expressed as

$$i^b_0 = i'^b_0 C, \tag{16}$$

where C is the bulk concentration of the reacting species, and given that the limiting current density is given by

$$i_L = zFkC, \tag{17}$$

then the expression for the cathodic reaction rate with explicit reactant concentrations is

$$|i_c| = \frac{i'^b_{0,c} C^2_{Cu^{2+}} z_c F k_c}{i'^b_{0,c} C_{Cu^{2+}} + z_c F k_c C_{Cu^{2+}} \exp\left(\dfrac{\alpha_c F}{GT}\eta_c\right)} \tag{18}$$

and for the anodic reaction:

$$i_a = \frac{i'^b_{0,a} C^2_{Fe^{2+}} z_a F k_a}{i'^b_{0,a} C_{Fe^{2+}} + z_a F k_a C_{Fe^{2+}} \exp\left(\dfrac{-\alpha_a F}{GT}\eta_a\right)}. \tag{19}$$

For secondary reactions, i.e., hydrogen ion reduction to gaseous hydrogen at the cathode and water oxidation to gaseous oxygen at the anode, Tafel kinetics (high-field approximations to the Butler–Volmer equation) were used to calculate the reaction rates, as they are controlled by charge transfer in the studied potential range.

$$i_{a,s} = i^{sf}_{0,a,s} \exp\left(\frac{\alpha_{a,s} F}{GT}\eta_{a,s}\right), \tag{20}$$

$$|i_{c,s}| = i^{sf}_{0,c,s} \exp\left(\frac{-\alpha_{c,s} F}{GT}\eta_{c,s}\right). \tag{21}$$

The cell voltage is

$$V_{cell} = \Delta E_e + \eta_a + |\eta_c| + I(R_a + R_c + R_m), \tag{22}$$

where $\Delta E_e = E_{e,a} - E_{e,c}$.

The electrical resistances of anolyte and catholyte are given by

$$R = \frac{1}{\kappa}\frac{d}{A}. \tag{23}$$

Ohm's law provides a relationship between current density and potential gradient:

$$i = -\kappa \nabla \Phi \tag{24}$$

and the electroneutrality condition is

$$\sum C_j z_j = 0. \tag{25}$$

The electrical conductivity of concentrated electrolytes is given by

$$\kappa = \frac{F^2}{GT} \sum z_j^2 C_j D_{ef,j}, \tag{26}$$

where the effects of concentration are represented by effective diffusivities (D_{ef}), i.e., diffusivities whose values are calculated so as to make Eq. (26) valid for concentrated electrolytes (Cifuentes et al., 2007). They are determined by a procedure proposed by Anderko et al. (1997) and Casas et al. (2000, 2005a) based on measurements of the electrical conductivity of the solutions of interest. Values for effective diffusivities used by the present model are given below.

Faraday's law links current density to ion flux as

$$i = F \sum z_j N_j. \tag{27}$$

The membrane resistance (R_m) was calculated from a mass balance of charged species in anolyte and catholyte assuming: (a) electroneutrality in both electrolytes and (b) that H^+ transports through the membrane only by diffusion whereas sulphate

transports only by migration (Lorrain et al., 1996, 1997; Lott et al., 2005). Effective diffusivities were used for H^+ and sulphate transport through the membrane. The resulting expression is

$$R_m = \frac{GTV_a x_m \left(C_{\text{tot}} - \dfrac{n}{V_a} \right)}{IFA_m t 2 D_{\text{ef},H^+} z_{\text{sulphate}} \bar{C}_{\text{sulphate}}}. \quad (28)$$

3.3. Transport phenomena

Taking into account the migration and diffusion phenomena, the transport flux through the membrane for concentrated electrolytes is given by (Newman, 1967)

$$N_{j,m} = N_{j,\text{mig}} + N_{j,\text{dif}} = -\frac{z_j F}{GT} D_{\text{ef},j} C_{j,m} \frac{\Delta\Phi}{\Delta x} - D_{\text{ef},j} \frac{\Delta C_j}{\Delta x}. \quad (29)$$

As in the case of the electrical conductivity of solutions (see above), the effects of concentration are represented by effective diffusivities.

Ion transport through anion membranes in sulphuric acid solutions has been studied by Lorrain et al. (1997).

The specific energy consumption is given by

$$\text{SEC} = \frac{V_{\text{cell}} I t}{m_{\text{Cu,dep}}}. \quad (30)$$

3.4. Concentration variations in the electrolytes

The copper mass deposited at the cathode per time unit is

$$\frac{\Delta m}{\Delta t} = \frac{i_c A_c}{z_c F}. \quad (31)$$

Copper concentration in the catholyte at time t_i is then

$$C_{Cu^{2+}}(t_i) = \frac{V_c C_{Cu^{2+}}(t_{i-1}) - \dfrac{i_c A_c}{z_c F} \Delta t}{V_c}. \quad (32)$$

Fe(II) and Fe(III) concentrations in the anolyte at time t_i are

$$C_{Fe^{2+}}(t_i) = \frac{V_a C_{Fe^{2+}}(t_{i-1}) - \dfrac{i_a A_a}{z_a F} \Delta t}{V_a}, \quad (33)$$

$$C_{Fe^{3+}}(t_i) = \frac{V_a C_{Fe^{3+}}(t_{i-1}) + \dfrac{i_a A_a}{z_a F} \Delta t}{V_a}. \quad (34)$$

3.5. Algorithm

The calculation starts with data input and then defines a temperature value and a time step. The latter determines the number of iterations to be carried out for a given cell operation time. For each iteration, the following calculations are performed at the chosen temperature: (a) speciation of anolyte and catholyte; (b) transport of ionic species through the membrane; (c) electrical conductivity of anolyte and catholyte; (d) anodic and cathodic overpotentials; (e) equilibrium potentials for electrode reactions; (f) cell voltage; (g) deposited copper mass; (h) produced amount of Fe(III) species; (i) mass balances for anolyte and catholyte. Then the time of operation is incremented by a time step (5 min) and the calculations are performed once again, taking into account the changes in the concentrations of reactants caused by the electrode reactions. The process is repeated until the total operation time is reached.

3.6. Model solution

The speciation of catholyte and anolyte at a given temperature was calculated using a set of non-linear equations, which is solved by an iterative algorithm which implements a Newton–Raphson method for a multi-dimensional system. Results from the speciation model were fed into a dynamic model of cell operation, which included calculations for both the electrode kinetics and the mass transport across the membrane at the defined temperature. Both models were coded using MATLAB V6.2 software (MATLAB, 2002) on a personal computer.

Kinetic parameters as functions of temperature were determined from experimental data; mixed control equations (18) and (19) were fitted to data for the main reactions and Tafel kinetics (Eqs. (20) and (21)) were fitted to data for secondary reactions. Other kinetic data have been published elsewhere (Cifuentes et al., 2004a, 2007; Casas et al., 2000, 2003, 2005a).

The sign convention used throughout states that cathodic overpotentials are negative and anodic overpotentials, positive.

3.7. Model calibration

The model was calibrated by experiment and curve fitting. The result was a set of relationships for catholyte and anolyte density, viscosity and electrical conductivity as functions of temperature.

3.8. Model validation

Model validation was achieved by carrying out four ad hoc experiments in the RED cell (at 45 and 55 °C and $i_{\text{cell}} = 300$ and 600 A/m^2), and comparing the results with the corresponding model calculations. The test variables were copper production rate, Fe(III) production rate, cell voltage and specific energy consumption. Operation parameters for the cell during the validation experiment (other than temperature and i_{cell}) were those in Table 1.

4. Results and discussion

4.1. Transport phenomena and electrode kinetics

Experimental results for density, viscosity and electrical conductivity of $CuSO_4$–H_2SO_4 and $FeSO_4$–H_2SO_4 solutions at several temperatures are presented in this section. Various mathematical functions were tested for the temperature dependence of each variable and the chosen relationships were the ones which produced the best correlation coefficients.

Table 4
Density (g/cm^3) of aqueous Cu–H_2SO_4 and Fe–H_2SO_4 solutions at 25 and 50 °C (298 and 323 K)

Temperature (°C)	25	50
Solution		
H_2SO_4 50 g/L	1.03	1.01
H_2SO_4 190 g/L	1.12	1.09
H_2SO_4 50 g/L, Cu 3 g/L	1.03	1.02
H_2SO_4 50 g/L, Cu 10 g/L	1.05	1.04
H_2SO_4 190 g/L, Cu 10 g/L	1.14	1.12
H_2SO_4 190 g/L, Cu 40 g/L	1.21	1.16
H_2SO_4 50 g/L, Fe 14 g/L	1.07	1.05
H_2SO_4 50 g/L, Fe 28 g/L	1.10	1.09
H_2SO_4 190 g/L, Fe 28 g/L	1.16	1.15
H_2SO_4 190 g/L, Fe 56 g/L	1.25	1.22

Table 5
Parameter values for the relationship between electrolyte density (g/cm^3), temperature (K) and concentrations (g/L) for catholyte and anolyte

Electrolyte	a_0	a_1	a_2	a_3	R^2
Anolyte	0.714	0.00058	0.00200	86.88	0.989
Catholyte	0.805	0.00053	0.00237	59.79	0.993

C_{Me}: concentration of Fe in anolyte or Cu in catholyte.
$\rho\ (\mathrm{g/cm^3}) = a_0 + \frac{a_1}{T\ (\mathrm{K})} + a_2 C_{H_2SO_4}\ (\mathrm{g/L}) + a_3 C_{Me}\ (\mathrm{g/L})$.

4.2. Density

Preliminary measurements showed that solution density varies linearly with temperature. Experimental results for the dependence of solution density on temperature and concentration are in Table 4.

The best fit for the obtained experimental results for both catholyte and anolyte was provided by the following relationship:

$$\rho\ (\mathrm{g/cm^3}) = a_0 + \frac{a_1}{T\ (\mathrm{K})} + a_2 C_{H_2SO_4}\ (\mathrm{g/L}) + a_3 C_{Me}\ (\mathrm{g/L}). \quad (35)$$

Table 5 shows the values of the a_0, a_1, a_2 and a_3 parameters for catholyte and anolyte, with the corresponding correlation coefficients. Parameter values were similar for both solutions and the correlation coefficients were about 0.99.

Figs. 2 and 3 show plots of catholyte and anolyte densities versus $1/T$ for various electrolyte concentrations.

4.3. Viscosity

Experimental results for the dependence of solution viscosity on temperature and concentration are in Table 6.

The best fit for the obtained experimental results for both catholyte and anolyte was provided by the following exponential relationship:

$$\mu\ (\mathrm{kg/m/s}) = [a_0 + a_1 C_{H_2SO_4}\ (\mathrm{g/L}) + a_2 C_{Me}\ (\mathrm{g/L})]e^{a_3/T\ (\mathrm{K})}. \quad (36)$$

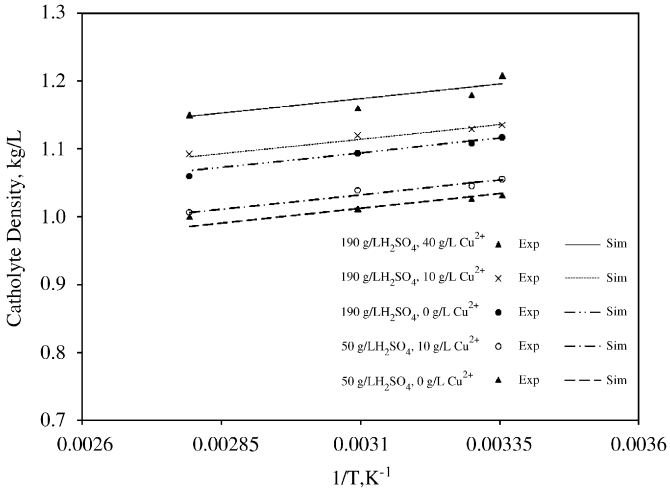

Fig. 2. Catholyte density as a function of temperature and concentration.

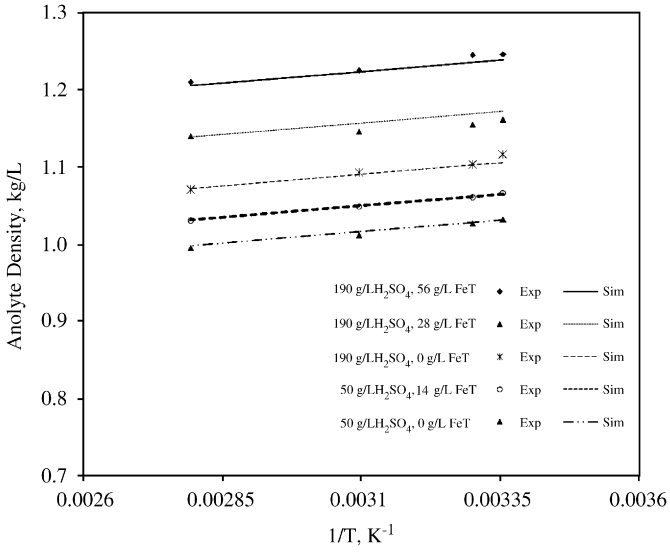

Fig. 3. Anolyte density as a function of temperature and concentration.

Table 6
Viscosity (kg/m/s × 10^4) of aqueous Cu–H_2SO_4 and Fe–H_2SO_4 solutions at various temperatures

Temperature (°C)	30	40	50	60
Solution				
H_2SO_4 50 g/L	8.2	6.8	5.6	4.9
H_2SO_4 190 g/L	10.4	8.5	7.3	6.0
H_2SO_4 50 g/L, Cu 3 g/L	8.8	7.1	6.0	5.4
H_2SO_4 50 g/L, Cu 10 g/L	9.1	7.4	6.0	5.8
H_2SO_4 190 g/L, Cu 10 g/L	12.0	9.9	8.0	7.1
H_2SO_4 190 g/L, Cu 40 g/L	13.3	11.0	8.9	7.8
H_2SO_4 50 g/L, Fe 14 g/L	10.1	8.2	6.8	6.0
H_2SO_4 50 g/L, Fe 28 g/L	11.0	8.9	7.4	6.7
H_2SO_4 190 g/L, Fe 28 g/L	12.7	10.5	8.4	7.5
H_2SO_4 190 g/L, Fe 56 g/L	16.4	13.6	11.0	9.8

Table 7 shows the values of the a_0, a_1, a_2 and a_3 parameters for catholyte and anolyte, with the corresponding correlation coefficients; the latter are about 0.99.

Table 7
Parameter values for the relationship between electrolyte viscosity (kg/m/s), temperature (K) and concentrations (g/L) for catholyte and anolyte

Electrolyte	a_0	a_1	a_2	a_3	R^2
Anolyte	2.26×10^{-6}	3.08×10^{-8}	4.19×10^{-9}	1759.99	0.990
Catholyte	1.92×10^{-6}	1.59×10^{-8}	4.23×10^{-9}	1813.02	0.986

C_{Me}: concentration of Fe in anolyte or Cu in catholyte.
μ (kg/m/s) $= [a_0 + a_1 C_{H_2SO_4}$ (g/L) $+ a_2 C_{Me}$ (g/L)$]e^{a_3/T\ (K)}$.

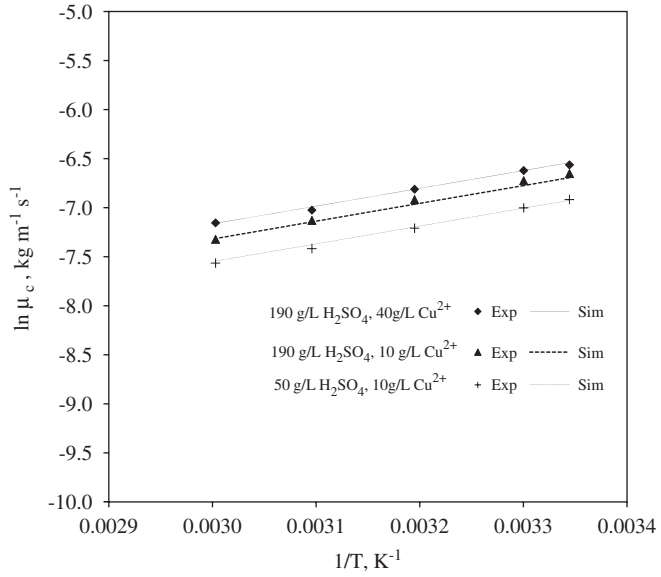

Fig. 4. Logarithm of catholyte viscosity versus $1/T$ at various concentrations.

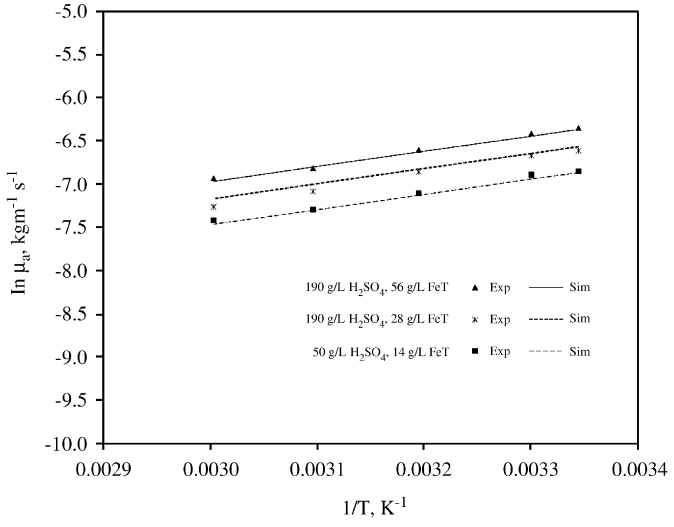

Fig. 5. Logarithm of anolyte viscosity versus $1/T$ at various concentrations.

Figs. 4 and 5 show logarithmic plots of the viscosity of catholyte and anolyte versus $1/T$ for various electrolyte concentrations.

4.4. Electrical conductivity

Experimental results for the dependence of the electrical conductivity of solutions on temperature and concentration are in Tables 8a and b.

Table 8
Electrical conductivity (Ω^{-1}m^{-1}) of aqueous (a) Cu–H_2SO_4 and (b) Fe–H_2SO_4 solutions at various temperatures

Temperature (°C)	[H_2SO_4] (g/L)	[Cu] (g/L)	Conductivity (Ω^{-1} m^{-1})
(a)			
30	0	0	0.020
30	100	0	27.80
30	200	0	62.00
30	50	10	14.47
30	200	40	71.00
40	0	0	0.022
40	100	0	27.70
40	200	0	65.00
40	50	10	18.80
40	200	40	74.00
50	0	0	0.023
50	100	0	31.80
50	200	0	68.00
50	50	10	19.90
50	200	40	76.30
55	0	0	0.024
55	100	0	32.50
55	200	0	69.50
55	50	10	23.30
55	200	40	77.80
Temperature (°C)	[H_2SO_4] (g/L)	[Fe] (g/L)	Conductivity (Ω^{-1} m^{-1})
(b)			
30	0	0	0.020
30	100	0	27.80
30	200	0	62.00
30	50	10	28.10
30	200	50	89.00
40	0	0	0.022
40	100	0	27.70
40	200	0	65.00
40	50	10	25.00
40	200	50	86.00
50	0	0	0.023
50	100	0	31.80
50	200	0	68.00
50	50	10	25.00
50	200	50	84.30
55	0	0	0.024
55	100	0	32.50
55	200	0	69.50
55	50	10	20.30
55	200	50	81.80

The best fit for the obtained experimental results for both catholyte and anolyte was provided by the following linear relationship:

$$\kappa\ (\Omega^{-1}\,\mathrm{m}^{-1}) = a_0 + a_1 C_{H_2SO_4}(\mathrm{g/L}) + a_2 C_{Me}\ (\mathrm{g/L}) + a_3 T(\mathrm{K}). \quad (37)$$

Table 9 shows the values of the a_0, a_1, a_2 and a_3 parameters for catholyte and anolyte, with the corresponding correlation coefficients. Parameter values are different for catholyte and anolyte and the correlation coefficient for the anolyte is smaller than for the catholyte.

Table 9
Parameter values for the relationship between electrolyte conductivity ($\Omega^{-1}\,m^{-1}$), temperature (K) and concentrations (g/L) for catholyte and anolyte

Electrolyte	a_0	a_1	a_2	a_3	R^2
Anolyte	34.06	0.3053	0.4159	−0.09676	0.978
Catholyte	−61.09	0.3211	0.2444	0.1941	0.995

C_{Me}: concentration of Fe in anolyte or Cu in catholyte.
$\kappa\ (\Omega^{-1}m^{-1}) = a_0 + a_1 C_{H_2SO_4}\ (g/L) + a_2 C_{Me}\ (g/L) + a_3 T\ (K)$.

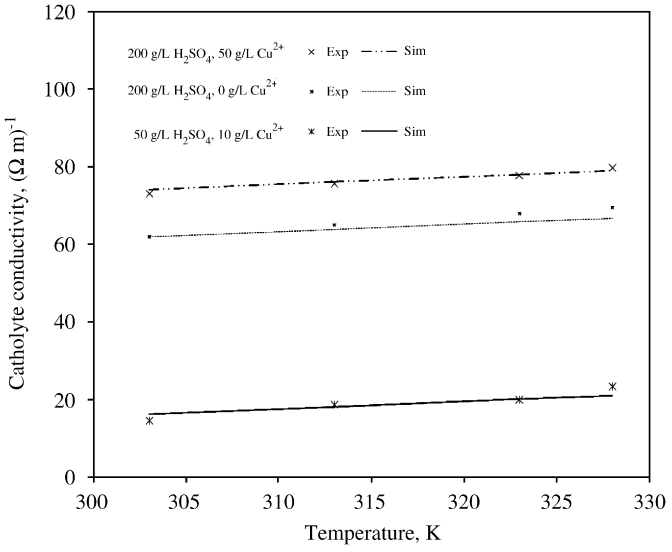

Fig. 6. Electrical conductivity of catholyte as a function of temperature and concentration.

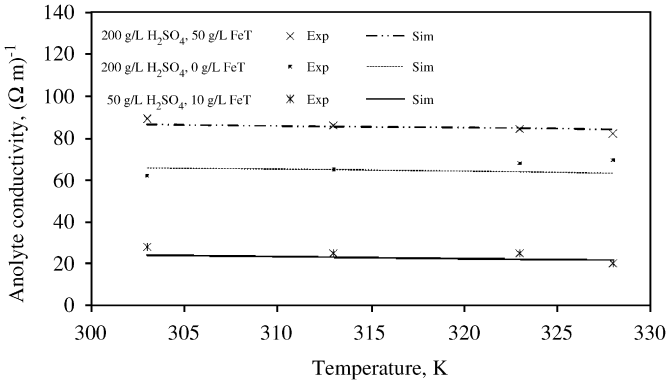

Fig. 7. Electrical conductivity of anolyte as a function of temperature and concentration.

Figs. 6 and 7 show linear plots of the electrical conductivity of catholyte and anolyte versus T for various electrolyte concentrations.

The conductivity of sulphuric acid clearly increases with temperature and so does the conductivity of Cu–H_2SO_4 solutions (see Tables 8a and b); however, the conductivity of Fe–H_2SO_4 solutions decreases with temperature. Price and Davenport (1981) showed that metals in hydrometallurgical solutions cause a decrease in the electrical conductivity. This is due to ion association to form more stable species, which diminishes the free H^+ concentration. Given that this ion exhibits the highest mobility and diffusivity (at least 5 times greater than any other cation in solution), its concentration decrease causes a solution conductivity drop. In the studied conditions, the effect of Fe is more pronounced that the effect of Cu, because Fe forms the stable $FeH(SO_4)_2$ species, whereas Cu does not form any H-containing species, in significant concentrations.

Table 10
Effective diffusivities of relevant ions inside the membrane as a function of temperature

T (°C)	D_{ef,H^+} (m^2/s)	$D_{ef,SO_4^{2-}}$ (m^2/s)
30	3.02×10^{-6}	5.25×10^{-8}
40	4.66×10^{-6}	7.05×10^{-8}
50	7.02×10^{-6}	9.30×10^{-8}
60	1.03×10^{-5}	1.21×10^{-7}

Table 11
Standard equilibrium constants of formation for species present in anolyte and catholyte between 25 and 65 °C

Species	Log K_f^0 25 °C	Log K_f^0 55 °C	Log K_f^0 45 °C	Log K_f^0 55 °C	Log K_f^0 65 °C
Anolyte					
HSO_4^-	1.98	2.12	2.26	2.36	2.52
$FeSO_4^0$	2.25	2.33	2.40	2.48	2.73
$Fe(SO_4)_2^-$	5.38	6.33	7.22	7.95	8.54
$FeSO_4^+$	4.04	4.34	4.63	4.91	5.20
$FeH(SO_4)_2^0$	8.10	8.90	9.70	10.60	11.60
Catholyte					
HSO_4^-	1.98	2.12	2.26	2.36	2.52
$CuSO_4^0$	2.36	2.46	2.56	2.63	2.74

4.5. Diffusivities

Effective diffusivities at 25 and 50 °C were estimated from published data (Casas et al., 2000, 2005a, b). Values at 30, 40 and 60 °C were determined using Arrhenius equation (Table 10).

4.6. Speciation of catholyte and anolyte

The temperature dependence of the speciation of Cu and Fe in sulphuric acid has been studied by Cifuentes et al. (2006). Values for equilibrium constants of formation for relevant catholyte and anolyte species are given in Table 11. The best fit for the temperature dependence of these constants was provided by the following logarithmic relationship:

$$\log(K_f^0) = a_0 + \frac{a_1}{T\ (K)} + a_2 \log(T\ (K)) + a_3 T\ (K). \qquad (38)$$

Table 12 shows the values of the parameters for all the relevant species plus the correlation coefficients. Results for the

speciation of anolyte and catholyte at 25, 35, 45, 55 and 65 °C are presented in Table 13. Both electrolytes exhibit high ionic strengths (about 3.2 m) and high association degrees between metallic ions and sulphate. Further details, concentration versus temperature plots and discussions regarding the temperature dependence of the speciation of the studied electrolytes can be found in Cifuentes et al. (2006).

4.7. Electrochemical kinetics

The temperature dependence of the cathodic and anodic kinetics in the RED cell has been studied by Cifuentes and Simpson (2005). Kinetic parameters at 30, 40, 50 and 60 °C, obtained by the methodology described in the above publication, are shown in Table 14. Table 15 shows results for secondary reactions.

Table 12
Parameter values for the relationship between the equilibrium constant of formation and temperature in catholyte and anolyte

Species	a_0	a_1	a_2	a_3	R^2
Anolyte					
HSO_4^-	0.3954	0.9962	−1.1263	0.0147	0.999
$FeSO_4^0$	0.8398	0.9990	−0.8950	0.0120	0.959
$Fe(SO_4)_2^-$	−1.9709	0.9812	−7.8709	0.0905	0.995
$FeSO_4^+$	0.0157	0.9938	−2.2090	0.0319	1.000
$FeH(SO_4)_2^0$	0.0118	0.9938	−3.7223	0.0981	0.997
Catholyte					
HSO_4^-	0.3954	0.9962	−1.1263	0.0147	0.999
$CuSO_4^0$	0.6184	0.9976	−0.4955	0.0100	0.998

$\log(K_f^0) = a_0 + \frac{a_1}{T\ (\mathrm{K})} + a_2 \log(T\ (\mathrm{K})) + a_3 T\ (\mathrm{K})$.

Fig. 8 is an Evans diagram which shows experimental results and fitted curves at 30, 40, 50 and 60 °C using the parameters in Table 14.

The best fit for the temperature dependence of the studied kinetic parameters was obtained with the following expressions (see Cifuentes and Simpson, 2005). For the exchange current density:

$$\ln(i_0^b, \mathrm{A/m^2}) = a_0 + \frac{a_1}{T\ (\mathrm{K})}. \tag{39}$$

For the limiting current density:

$$|i_L(\mathrm{A/m^2})| = a_0 + a_1 T\ (\mathrm{K}). \tag{40}$$

For the charge transfer coefficient:

$$\alpha = a_0 + a_1 T\ (\mathrm{K}) + a_2 [T\ (\mathrm{K})]^2. \tag{41}$$

Table 16 shows values for the i_0^b, i_L and α parameters as functions of temperature for the cathodic reactions and Table 17 does the same for the anodic reactions.

Plots for the temperature dependence of kinetic parameters and further discussions can be found in Cifuentes and Simpson (2005).

When the model used Eqs. (18) and (19) for determining reaction rates, the mass transfer coefficients (k_a, k_c) were calculated from limiting current density values obtained by Eq. (40).

4.8. Cell voltage

A comparison between measured and simulated cell voltages, with values for the components of the latter, is presented in Table 18a and b.

Table 13
Speciation of anolyte and catholyte at various temperatures

Species	Concentration (mol/kg)				
	25 °C	35 °C	45 °C	55 °C	65 °C
Anolyte					
H^+	1.2	1.16	1.12	1.10	1.08
SO_4^{2-}	1.35×10^{-1}	1.04×10^{-1}	7.88×10^{-2}	5.96×10^{-2}	4.49×10^{-2}
Fe^{2+}	7.17×10^{-1}	7.14×10^{-1}	7.13×10^{-1}	7.13×10^{-1}	7.14×10^{-1}
Fe^{3+}	5.81×10^{-7}	2.62×10^{-7}	3.63×10^{-8}	6.99×10^{-9}	$< 10^{-10}$
HSO_4^-	2.36	2.38	2.39	2.40	2.41
$FeSO_4^0$	2.35×10^{-1}	2.32×10^{-1}	2.28×10^{-1}	2.22×10^{-1}	2.17×10^{-1}
$Fe(SO_4)_2^-$	1.30×10^{-5}	1.55×10^{-5}	1.78×10^{-5}	1.68×10^{-5}	1.34×10^{-5}
$FeSO_4^+$	2.88×10^{-4}	1.98×10^{-4}	1.13×10^{-4}	4.04×10^{-5}	3.36×10^{-6}
$FeH(SO_4)_2^0$	2.77×10^{-2}	2.76×10^{-2}	2.74×10^{-2}	2.72×10^{-2}	2.71×10^{-2}
Ion strength	3.77	3.71	3.66	3.63	3.61
Catholyte					
H^+	1.57	1.53	1.50	1.47	1.44
SO_4^{2-}	8.99×10^{-2}	6.79×10^{-2}	5.10×10^{-2}	3.81×10^{-2}	2.84×10^{-2}
Cu^{2+}	3.26×10^{-1}	3.28×10^{-1}	3.30×10^{-1}	3.33×10^{-1}	3.36×10^{-1}
HSO_4^-	2.04	2.05	2.06	2.06	2.06
$CuSO_4^0$	1.13×10^{-1}	1.08×10^{-1}	1.02×10^{-1}	9.62×10^{-2}	9.04×10^{-2}
Ion strength	2.83	2.80	2.77	2.76	2.75

Anolyte composition: $[H_2SO_4] = 1.95$ m, $[Fe(II)] = 1.03$ m and $[Fe(III)] = 0.03$ m.
Catholyte composition: $[H_2SO_4] = 1.95$ m and $[Cu(II)] = 0.472$ m.

Table 14
Kinetic parameters for the main cathodic (Cu^{2+}/Cu^0) and anodic (Fe^{2+}/Fe^{3+}) reactions at various temperatures

Temperature (°C)	Cu^{2+}/Cu^0			Fe^{2+}/Fe^{3+}		
	α_c	$i_{0,c}$ (A/m^2)	$i_{L,c}$ (A/m^2)	α_a	$i_{0,a}$ (A/m^2)	$i_{L,a}$ (A/m^2)
30	0.95	0.8	318	0.51	2.8	423
40	1.01	4.5	448	0.64	3.4	648
50	1.05	78	694	0.71	4.4	761
60	1.10	825	746	0.78	6.2	842

Table 15
Kinetic parameters for parasitic cathodic (H^+/H_2) and anodic (H_2O/O_2) reactions at various temperatures

Temperature (°C)	H^+/H_2		H_2O/O_2	
	α_{pc}	i_{0pc} (A/m^2)	α_{pa}	i_{0pa} (A/m^2)
30	NO	NO	0.10	0.11
40	NO	NO	0.11	0.50
50	NO	NO	0.10	0.88
60	0.05	691	0.10	1.55

NO = reaction not observed.

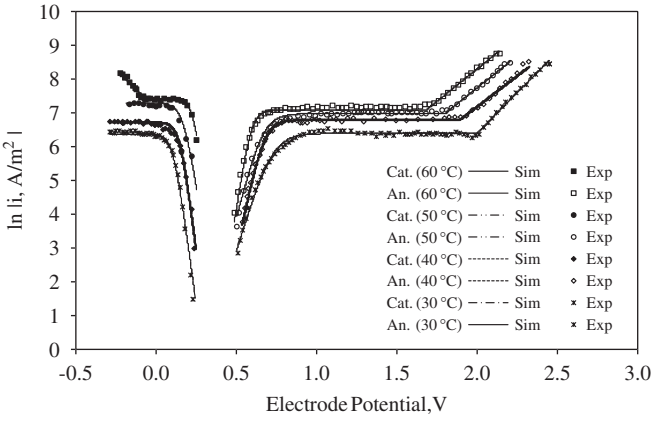

Fig. 8. Evans diagram showing experimental results and fitted curves for potentiodynamic sweeps. Cathodic reactions are copper deposition and hydrogen evolution. Anodic reactions are Fe(II) oxidation and oxygen evolution.

Table 16
Parameter values (a_0, a_1, a_2) for the relationship between kinetic parameters and temperature for Cu^{2+}/Cu^0

Relationship	a_0	a_1	a_2	R^2
$\alpha_c = a_0 + a_1 T(\mathrm{K}) + a_2[T(\mathrm{K})]^2$	−0.537	0.0049	0	0.998
$\ln(i_{0,c}, \mathrm{A/m^2}) = a_0 + \frac{a_1}{T(\mathrm{K})}$	78.27	−23878	–	0.978
$\lvert i_{L,c}\ (\mathrm{A/m^2})\rvert = a_0 + a_1 T\ (\mathrm{K})$	−4601	16.32	–	0.958

Table 17
Parameter values (a_0, a_1, a_2) for the relationship between kinetic parameters and temperature for Fe^{2+}/Fe^{3+}

Relationship	a_0	a_1	a_2	R^2
$\alpha_a = a_0 + a_1 T(\mathrm{K}) + a_2[T(\mathrm{K})]^2$	0.994	−0.017	$5.16 \times 10^{-0.5}$	0.973
$\ln(i_{0,a}, \mathrm{A/m^2}) = a_0 + \frac{a_1}{T(\mathrm{K})}$	21.78	−6647	–	0.980
$\lvert i_{L,a}\ (\mathrm{A/m^2})\rvert = a_0 + a_1 T(\mathrm{K})$	−2267	8.44	–	0.965

Table 18
(a) Experimental and simulated cell voltage (V_{cell}) and (b) values for simulated components of cell voltage

T (°C)	i_{cell} (A/m^2)	Experim. V_{cell} (V)	Simul. V_{cell} (V)	Error (%)
(a)				
30	253	1.01	1.03	2.30
30	435	2.20	2.28	3.64
30	572	2.40	2.37	1.29
40	370	1.10	1.11	0.67
40	450	2.10	2.10	0.10
40	600	2.25	2.22	1.33
50	342	0.72	0.73	1.07
50	450	1.02	0.99	2.80
50	600	2.00	2.02	1.09
60	300	0.67	0.63	5.59
60	381	0.74	0.70	5.55
60	450	0.80	0.76	4.76

T (°C)	i_{cell} (A/m^2)	ΔE_e (V)	η_a (V)	$\lvert\eta_c\rvert$ (V)	IR_a (V)	IR_c (V)	IR_m (V)
(b)							
30	253	0.287	0.405	0.203	0.038	0.040	0.058
30	435	0.301	1.553	0.238	0.065	0.068	0.061
30	572	0.309	1.600	0.240	0.080	0.080	0.062
40	370	0.303	0.493	0.146	0.052	0.053	0.061
40	450	0.309	1.429	0.170	0.063	0.065	0.062
40	600	0.317	1.487	0.184	0.084	0.086	0.065
50	342	0.307	0.209	0.058	0.045	0.046	0.063
50	450	0.314	0.396	0.084	0.066	0.067	0.064
50	600	0.323	1.358	0.114	0.079	0.080	0.067
60	300	0.308	0.153	0.007	0.050	0.050	0.063
60	381	0.315	0.175	0.018	0.063	0.063	0.065
60	450	0.323	0.202	0.028	0.075	0.075	0.066

The relative error is between 0.1 and 5.6%.

The mixed control equations are valid, in principle, for overpotentials whose absolute values are higher than 0.1 V. Tables 18a and b show that, out of 24 calculated overpotential values, five (all cathodic) are predicted as being less than 0.1 V. For these values there should be a greater error than for the rest of them and this seems to be confirmed by the fact that the greatest errors for the cell voltage occur in three out of these five cases. In a strict sense, for these five cases, the overpotentials should be calculated by the Butler–Volmer equation and not by the mixed control equations (18) and (19), but the results' error is less than 5.6% in all cases.

In Table 18b it is clear that there is a slight increase in IR values with increasing temperature. This is the opposite

Table 19
Model validation[a]

Variable	Unit	$i_{cell} = 300\,A/m^2$			$i_{cell} = 600\,A/m^2$		
		Experimental	Simulated	Error (%)	Experimental	Simulated	Error (%)
Copper production	kg/h	1.38×10^{-4}	1.40×10^{-4}	0.94	2.77×10^{-4}	2.80×10^{-4}	1.01
Fe(III) production	kg/h	2.45×10^{-4}	2.46×10^{-4}	0.43	4.88×10^{-4}	4.92×10^{-4}	0.94
Average cell voltage	V	0.77	0.80	3.77	2.23	2.26	1.39
Specific energy consumption	kWh/kg Cu	0.67	0.69	2.42	1.93	1.94	0.38

Experimental and simulated results at 45 °C.
[a]Cell operation parameters are shown in Table 1.

Table 20
Model validation[a]

Variable	Unit	$i_{cell} = 300\,A/m^2$			$i_{cell} = 600\,A/m^2$		
		Experimental	Simulated	Error (%)	Experimental	Simulated	Error (%)
Copper production	kg/h	1.41×10^{-4}	1.40×10^{-4}	0.99	2.84×10^{-4}	2.80×10^{-4}	1.55
Fe(III) production	kg/h	2.40×10^{-4}	2.46×10^{-4}	2.52	4.83×10^{-4}	4.92×10^{-4}	1.99
Average cell voltage	V	0.67	0.69	3.43	1.94	1.94	0.15
Specific energy consumption	kWh/kg Cu	0.47	0.50	4.47	1.64	1.67	1.73

Experimental and simulated results at 55 °C.
[a]Cell operation parameters are shown in Table 1.

of what should be expected. The reason for this unexpected prediction may be that there are additional IR drops which have not been included in the present model. One of such drops may be caused by an increase in the concentration polarization in the zone adjacent to the membrane. This would be caused by an increase in the local concentration of cations, which, in turn, could be influenced by an increase in cation transport rates at higher temperatures. Speciation may also play a role, as an increased temperature causes a greater concentration of ferric ion and, subsequently, an increase in the formation of ions such as $Fe(SO_4)_2^-$ and $FeSO_4^+$, which are not considered in the present model of the electrical conductivity; only total Fe and Fe(II) concentrations are included. As will be shown in Section 4.9, these weaknesses in the model did not hinder its validation.

4.9. Model validation

Model validation was achieved by carrying out four ad hoc experiments in the RED cell (at 45 and 55 °C and $i_{cell} = 300$ and $600\,A/m^2$), and comparing the results with the corresponding model calculations. Tables 19 and 20 show measured and calculated values for Cu and Fe(III) production rates, average cell voltage and specific energy consumption. Other RED cell operation parameters are in Table 1.

Table 19 shows that, at 45 °C, the relative errors for model predictions are greater at $600\,A/m^2$ than the errors at $300\,A/m^2$. On the other hand, Table 20 demonstrates that, at 55 °C, most of the errors at $300\,A/m^2$ are greater than the errors at $600\,A/m^2$. It is also worth noting that, at 45 °C, prediction errors range from 0.43% to 3.77%, whereas at 55 °C, they range from 0.15% to 4.47%.

4.9.1. Copper production

The cathodic current efficiency was calculated as

$$\eta_{curr} = \frac{m_{Cu,dep}}{m_{Cu,calc}} \times 100. \quad (42)$$

Tables 19 and 20 show that the relative error for the predicted value of this parameter was between 0.94% and 1.55%.

Fig. 9 shows the dependence on time of the concentration of copper species in the catholyte and of the mass of deposited copper, as predicted by the model at 45 °C. During the operation, copper is deposited on the cathode and the concentration of copper-containing species in the catholyte decreases with time.

4.9.2. Production of ferric species

Fig. 10 shows the dependence on time of the concentration of Fe(II) and Fe(III) species as predicted by the model at 45 °C. During the operation, Fe(II) species are continuously oxidized at the anode so that the concentration of Fe(III) species in the anolyte increases with time, whereas the concentration of Fe (II) species decreases. The prediction error for this variable ranged from 0.43% to 2.52%.

4.9.3. Cell voltage as a function of time

The variation of the cell voltage with time at 45 and 55 °C, for cell current densities of 300 and $600\,A/m^2$ in 4 h runs,

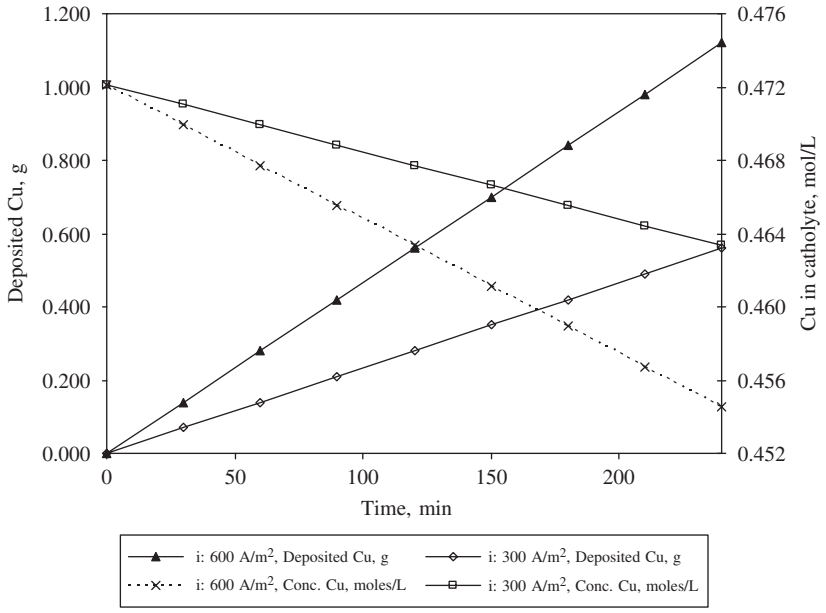

Fig. 9. Mass of deposited copper and copper concentration in the catholyte versus time of cell operation at 45 °C for two different cell current densities (simulated results).

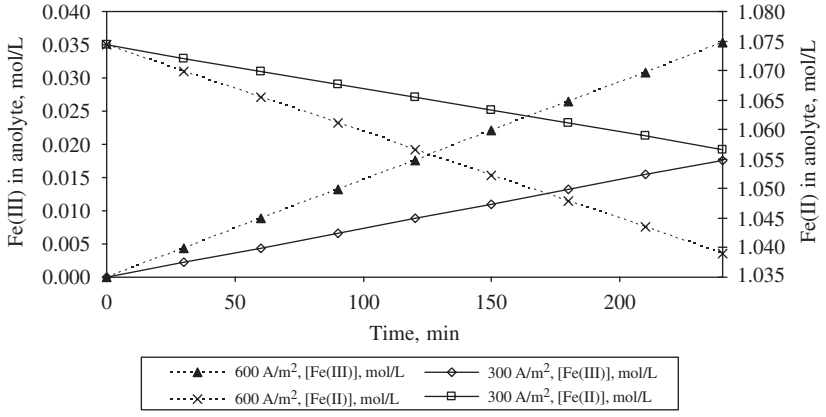

Fig. 10. Fe(II) and Fe(III) concentrations in the anolyte versus time of cell operation at 45 °C for two different cell current densities (simulated results).

is given in Fig. 11. Initially, the model overestimated the cell voltage by up to 8% (in the 45 °C, 600 A/m^2 case), but after 5–10 min of cell operation time (depending on conditions), the predicted value came close to the measured value. From then on, the simulated and experimental values were similar, with a relative error between 0.1% and 5.6% for the predicted average cell voltage (Tables 19 and 20).

4.9.4. Specific energy consumption

Tables 19 and 20 show that the difference between simulation and experiment for specific energy consumption was between 0.38% and 4.47%.

4.10. Temperature and cell optimization

Both the cell voltage and the specific energy consumption fall (i.e., improve) with increasing temperature. These results suggest that cell could be optimized by increasing its operation temperature. However, there are limitations to the increase of this variable due to the fact that it would imply: (a) higher heating costs; (b) higher water evaporation rate (i.e., increased water loss); (c) reduced lifespan for membranes and other temperature-sensitive cell materials. The maximum temperature at which an industrial RED cell could be practically operated should be determined by long-term pilot-scale tests.

4.11. Further work

Modelling work continues on the effect of geometrical changes on RED cell performance. This is being carried out with a finite elements code. The 2-D and 3-D models are being developed. These models will use results from the present model as input data.

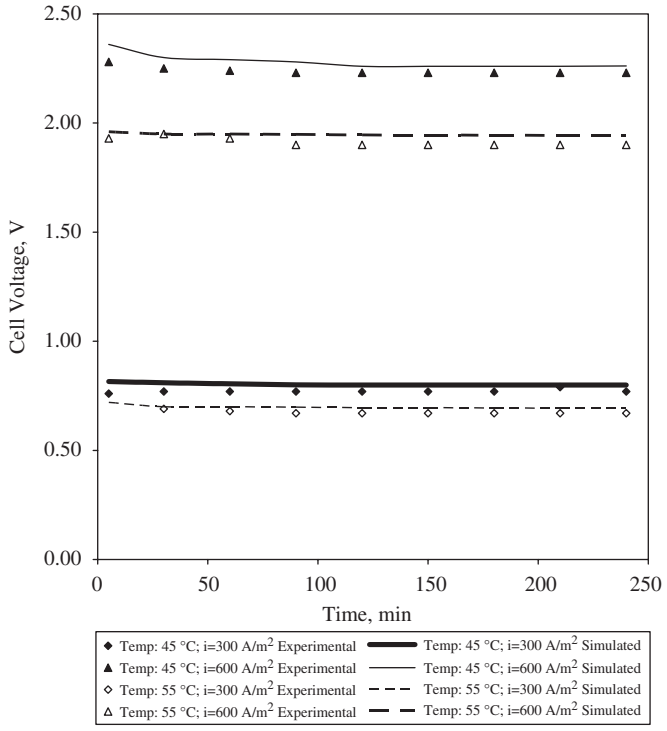

Fig. 11. Measured and simulated cell voltages versus time of cell operation.

5. Conclusions

(1) In the studied conditions, it is possible to simulate the behaviour of a lab-scale copper electrowinning cell based on reactive electrodialysis using a dynamic (time-dependent) and temperature-dependent mathematical model which includes the cathodic and anodic electrochemical kinetics, the transport phenomena in catholyte and anolyte, the speciation of these solutions and ion transport through the membrane.

(2) Agreement between experiment and model prediction is good for copper production rate, Fe(III) production rate, cell voltage and specific energy consumption within the studied temperature range.

(3) The main effects of increasing temperature on the performance of the RED cell are clearly to decrease the average cell voltage and the specific energy consumption. At the same time, the copper production rate increased slightly with increasing temperature.

(4) The developed model, if used jointly with 2-D or 3-D models, could be useful to assist in the design and operation of copper electrowinning cells based on reactive electrodialysis in the 30–60 °C and 250–600 A/m^2 ranges.

Notation

a	anodic subindex
a, s	anodic subindex for a secondary reaction
a_j	parameters in Eqs. (35)–(41)
A	cross-sectional area perpendicular to ion flow, m^2
A_a, A_c, A_m	surface area of anode, cathode and membrane, m^2
A_γ	Debye–Hückel parameter, $kg^{0.5}/mol^{0.5}$
B_γ	Debye–Hückel parameter, $kg^{0.5}/mol^{0.5}/Å$
$\dot{B}$	B-dot parameter, kg/mol
c	cathodic subindex
c, s	cathodic subindex for a secondary reaction
C, C_{Cu}^{2+}, C_{Fe}^{2+}	concentration of ionic species, mol/L
C_{Me}	metal concentration, g/L
$\bar{C}_{sulphate}$	average sulphate concentration (anolyte and catholyte), mol/L
C_{tot}	total concentration of charged species in anolyte, mol/L
d	distance travelled by ions, m
D_{ef}	effective diffusivity, m^2/s
$E_{e,a}$	equilibrium potential, main anodic reaction, V
$E_{e,c}$	equilibrium potential, main cathodic reaction, V
ΔE_e	difference between the equilibrium potentials of the mainreactions, V
F	Faraday constant, C/eq
G	gas constant, J/mol/K
i, i_a, i_c	current density, anodic and cathodic, A/m^2
i_L, $i_{L,a}$, $i_{L,c}$	limiting current density, anodic and cathodic, A/m^2
i_0^b, $i_{0,a}^b$, $i_{0,c}^b$	exchange current density, anodic and cathodic reactions, in terms of reactant concentrations in the bulk solution, A/m^2
$i_0'^b$	modified exchange current density, $A/m^2\,L/mol$
i_0^{sf}	exchange current density in terms of reactant concentrations at the electrode surface, A/m^2
I	cell current, A
I_γ	ionic strength, mol/kg
j	species subindex
k, k_a, k_c	mass transfer coefficient, anodic and cathodic, m/s
K_f^0	equilibrium constant of formation
m	membrane subindex
$m_{Cu,dep}$	experimentally determined deposited copper mass, kg
$m_{Cu,calc}$	deposited copper mass calculated by Faraday's law, kg
Δm	reacted mass in a time interval Δt, kg
N	ionic flux, $mol/m^2/s$
N_{dif}	diffusion flux, $mol/m^2/s$
N_{mig}	migration flux, $mol/m^2/s$
r	ionic radius, m
R_a, R_c, R_m	electrical resistance of anolyte, catholyte and membrane, Ω
t	time, s
T	temperature, K
Δt	time interval, s
V_a,V_c	volume of anolyte, catholyte, m^3
V_{cell}	cell voltage, V
x	distance, m
x_m	membrane thickness, m
z, z_a, z_c	charge number, anodic and cathodic reactions
$z_{sulphate}$	charge number for sulphate ion

Greek letters

α_a, α_c	anodic and cathodic charge transfer coefficients

$\gamma_{\pm}$	mean activity coefficient
η, η_a, η_c	overpotential, anodic and cathodic, V
η_{curr}	current efficiency, %
κ	electrical conductivity, $\Omega^{-1}\,\text{m}^{-1}$
μ	viscosity of electrolyte, kg/m/s
ρ	density, kg/m^3
Φ	inner or Galvani potential, V

Acknowledgements

This work was funded by the National Committee for Science and Technology (CONICYT, Chile) via FONDECYT project no. 101 0138. Thanks are due to Gloria Crisóstomo, Rodrigo Ortiz, Daniel Guerra and Juan Luis Yarmuch for their help with the experimental work. The continued support from the Departments of Mining Engineering, Universidad de Chile, and Metallurgical Engineering, Universidad de Santiago, are gratefully acknowledged.

References

Bockris, J.O'M., Reddy, A.K.N., 2000. Modern Electrochemistry, vol. 2. Plenum Press, New York, USA.

Casas, J.M., Alvarez, F., Cifuentes, L., 2000. Aqueous speciation of sulfuric acid—cupric sulphate solutions. Chemical Engineering Science 55, 6223–6234.

Casas, J.M., Crisóstomo, G., Cifuentes, L., 2003. Aqueous speciation of electrowinning solutions. In: Riveros, P.A., Dixon, D., Dreisinger, D.B., Menacho, J., (Eds.), Proceedings of the Copper 2003, International Conference, Santiago, Chile, November 30th–December 3rd, 2003. Hydrometallurgy of Copper, vol. VI, Book 1, Canadian Institute of Mining, Metallurgy and Petroleum, pp. 441–456.

Casas, J.M., Crisóstomo, G., Cifuentes, L., 2005a. Aqueous speciation of the Fe(II)–Fe(III)–H_2SO_4 system at 25 and 50 °C. Hydrometallurgy 80 (4), 254–264.

Casas, J.M., Papangelakis, V.G., Liu, H., 2005b. Performance of three chemical models on the high temperature aqueous $Al_2(SO_4)_3$–$MgSO_4$–H_2SO_4–H_2O system. Industrial and Engineering Chemistry Research 44 (9), 2931–2941.

Cifuentes, L., Simpson, J., 2005. Temperature dependence of the cathodic and anodic kinetics in a copper EW cell based on reactive electrodialysis. Chemical Engineering Science 60 (17), 4915–4923.

Cifuentes, L., Crisóstomo, G., Ibáñez, J.P., 2002. On the electrodialysis of aqueous H_2SO_4–$CuSO_4$ electrolytes with metallic impurities. Journal of Membrane Science 207, 1–16.

Cifuentes, L., Glasner, R., Casas, J.M., 2004a. Aspects of the development of a copper electrowinning cell based on reactive electrodialysis. Chemical Engineering Science 59 (5), 1087–1101.

Cifuentes, L., Mondaca, C., Casas, J.M., 2004b. The effectiveness of membrane systems for the separation of anolyte and catholyte in a lab-scale copper electrowinning cell based on reactive electrodialysis. Minerals Engineering 17, 803–809.

Cifuentes, L., Ortiz, R., Casas, J.M., 2005. Electrowinning of copper in a lab-scale squirrel-cage cell with anion membrane. A.I.Ch.E. Journal 51 (8), 2273–2284.

Cifuentes, L., Casas, J.M., Simpson, J., 2006. Temperature dependence of the speciation of Cu and Fe in acidic electrolytes. Chemical Engineering Research and Design 84 (A10), 965–969.

Cifuentes, L., Castro, J.M., Casas, J.M., Simpson, J., 2007. Modelling a copper electrowinning cell based on reactive electrodialysis. Applied Mathematical Modelling 31 (7), 1308–1320.

Helgeson, H.C., 1969. Thermodynamics of hydrothermal systems at elevated temperatures and pressures. American Journal of Science 267, 724–804.

Lorrain, Y., Pourcelly, G., Gavach, C., 1996. Influence of cations on the proton leakage through anion exchange membranes. Journal of Membrane Science 110, 181–190.

Lorrain, Y., Pourcelly, G., Gavach, C., 1997. Transport mechanism of sulfuric acid through an anion exchange membrane. Desalination 109, 231–239.

Lott, K., Ghosh, B., Ritchiez, J., 2005. Measurement of anion diffusion and transference numbers in an anhydrous proton conducting electrolyte. Electrochemical and Solid-State Letters 8, A513–A515.

MATLAB, MATLAB Mathematical Software, 2002. Version 6.2. The Math Works Inc.: 24 Prime Park Way, Natick, MA 01760-1500, USA. ⟨www.mathworks.com⟩.

Newman, J., 1967. Transport processes in electrolytic solutions, In: Tobias, C.W., (Ed.), Advances in Electrochemistry and Electrochemical Engineering. New York, USA, pp. 87–135.

Price, D., Davenport, W., 1981. Physico-chemical properties of copper electrorefining and electrowinning electrolytes. Metallurgical Transactions B 12B, 639–643.